Journal of Colloid and Interface Science 657 (2024) 778–787

Contents lists available at ScienceDirect

Journal of Colloid And Interface Science

journal homepage: www.elsevier.com/locate/jcis

The efficient magneto-mechanical actuation of cancer cells using a very low concentration of non-interacting ferrimagnetic hexaferrite nanoplatelets

Tanja Goršak [a,b], Eva Jarc Jovičić [b,c], Larisa Tratnjek [d], Igor Križaj [c], Borja Sepulveda [e], Josep Nogues [f,g], Mateja Erdani Kreft [d], Toni Petan [c], Slavko Kralj [a], Darko Makovec [a,b,*]

[a] Department for Materials Synthesis, Jožef Stefan Institute, Jamova 39, SI-1000 Ljubljana, Slovenia
[b] Jožef Stefan International Postgraduate School, Jamova 39, SI-1000 Ljubljana, Slovenia
[c] Department of Molecular and Biomedical Sciences, Jožef Stefan Institute, Jamova cesta 39, Ljubljana SI-1000, Slovenia
[d] University of Ljubljana, Faculty of Medicine, Institute of Cell Biology, Vrazov trg 2, 1000 Ljubljana, Slovenia
[e] Instituto de Microelectronica de Barcelona (IMB-CNM, CSIC), Campus UAB, 08193 Bellaterra, Barcelona, Spain
[f] Catalan Institute of Nanoscience and Nanotechnology (ICN2), CSIC and BIST, Campus UAB, Bellaterra, E-08193 Barcelona, Spain
[g] ICREA, Pg. Lluís Companys 23, 08010 Barcelona, Spain

GRAPHICAL ABSTRACT

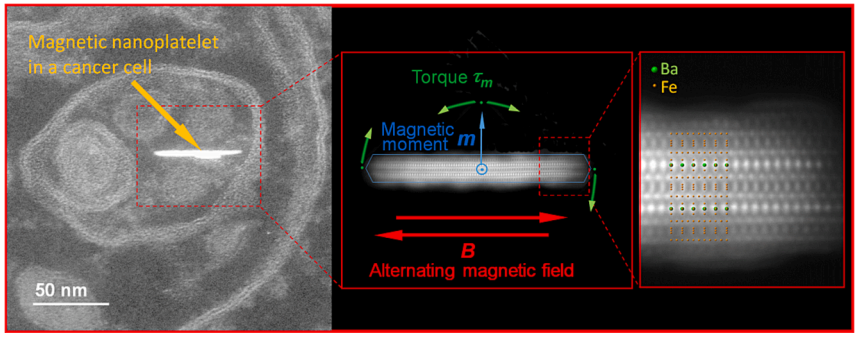

ARTICLE INFO

Keywords:
Magneto-mechanical actuation
Hexaferrite nanoplatelets
Cancer
Cell viability
Colloidal stability

ABSTRACT

Magneto-mechanical actuation (MMA) using the low-frequency alternating magnetic fields (AMFs) of magnetic nanoparticles internalized into cancer cells can be used to irreparably damage these cells. However, nanoparticles in cells usually agglomerate, thus greatly augmenting the delivered force compared to single nanoparticles. Here, we demonstrate that MMA also decreases the cell viability, with the MMA mediated by individual, non-interacting nanoparticles. The effect was demonstrated with ferrimagnetic (i.e., permanently magnetic) barium-hexaferrite nanoplatelets (NPLs, ~50 nm wide and 3 nm thick) with a unique, perpendicular orientation of the magnetization. Two cancer-cell lines (MDA-MB-231 and HeLa) are exposed to the NPLs *in-vitro* under different cell-culture conditions and actuated with a uniaxial AMF. TEM analyses show that only a small number of NPLs internalize in the cells, always situated in membrane-enclosed compartments of the endosomal-lysosomal system. Most compartments contain 1–2 NPLs and only seldom are the NPLs found in small groups, but never in close contact or mutually oriented. Even at low concentrations, the single NPLs reduce the cell viability

* Corresponding author.
E-mail address: Darko.Makovec@ijs.si (D. Makovec).

https://doi.org/10.1016/j.jcis.2023.12.019
Received 10 October 2023; Received in revised form 24 November 2023; Accepted 3 December 2023
Available online 4 December 2023

when actuated with AMFs, which is further increased when the cells are in starvation conditions. These results pave the way for more efficient *in-vivo* MMA at very low particle concentrations.

1. Introduction

Different therapeutic, diagnostic and theranostic approaches have been proposed based on magnetic nanoparticles (MNPs) in applied magnetic fields. For example, a magnetic field gradient can be used to concentrate the MNPs in a certain part of the human body (magnetic targeting, e.g., for targeted drug delivery) [1–3]. The MNPs can be remotely actuated with an alternating magnetic field to transfer the mechanical forces (magneto-mechanical actuation, MMA) [4–8] or heat (magnetic hyperthermia) [9] to biological structures, while the location of the MNPs in a particular tissue can be detected using magnetic resonance imaging [10] or magnetic particle imaging [11,12] (for diagnostics). In recent years, MMA has been proposed as an alternative cancer treatment, with high hopes of overcoming some of the limitations of current, targeted therapies, such as drug resistance and relapse through molecular, oncogene-driven signalling and the metabolic adaptations of cancer cells within heterogeneous tumour formations [5]. The MMA treatment is based on the localized, subcellular transfer of minute mechanical forces from the MNPs (sometimes referred to as magnetic nanomotors) to different cellular structures to cause irreparable damage and induce cell death. The MMA of magnetic nanoparticles can also be used to remotely trigger release of therapeutic agents from micro- and nanoscale delivery systems [13,14]. The force originates from the oscillatory motion of the MNPs synchronized with an applied, low-frequency, alternating magnetic field (AMF, frequency $<\sim$1 kHz). In a non-uniform AMF, the temporal variations of the magnetic field gradients will cause a lateral, vibration-like oscillatory motion of the MNPs, i.e., the MNP will be pulled towards the alternating direction of the regions with a larger field. In a spatially homogeneous AMF, a MNP will experience rotation, because it will tend to align its magnetic moment with the applied field (see sketch in Fig. 1(a)). Importantly, this physical rotation will only be active for the MNPs exhibiting a high enough magnetic anisotropy energy; high enough to prevent magnetization reversal within the particle [6–8]. Note that superparamagnetic NPs, which are frequently applied in medicine [1], will only rotate effectively in a rotating magnetic field when they have an anisotropic shape [6–8,15]. The force $\boldsymbol{F_m}$ that can be produced by the MMA depends on the characteristics of the MNPs (their size, shape, and magnetic properties) and the type and characteristics of the AMF (amplitude $\boldsymbol{B}$, frequency ω, uniaxial, rotating, vibrating, pulsed, chaotic,

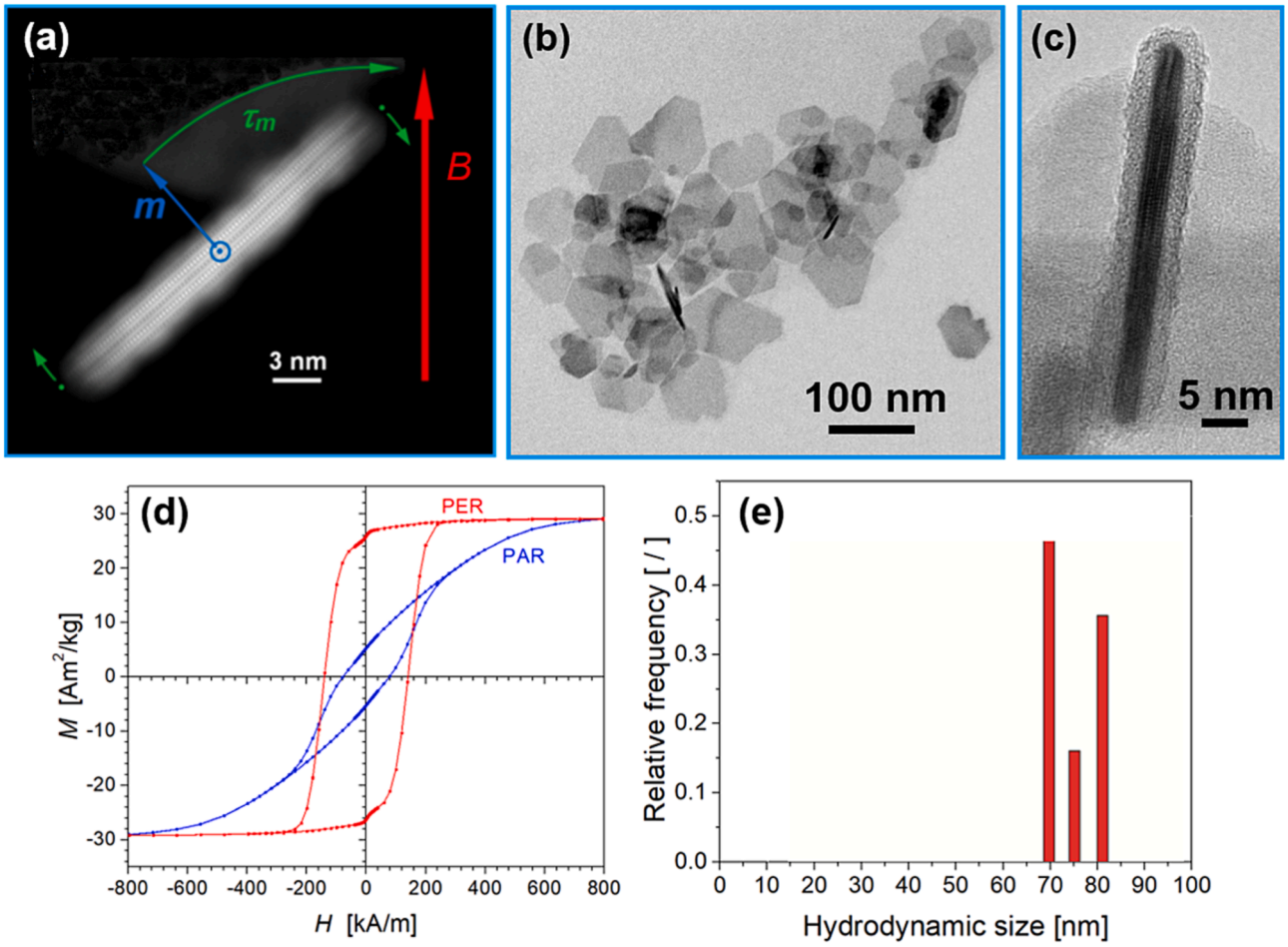

Fig. 1. (a) Atomic-resolution HAADF-STEM image of NPL oriented edge-on, with a schematic of the direction of its magnetic moment $\boldsymbol{m}$ and its response to a magnetic field. The magnetic moment of the particle tends to align with the direction of the applied magnetic field $\boldsymbol{B}$, resulting in the NPL's rotation and transfer of the driving torque $\boldsymbol{\tau_m}$ to the NPL's surroundings. (b) TEM image of NPLs oriented in-plane. (c) TEM image of a silica-coated NPL oriented edge-on. The image shows that the silica layer is amorphous. (d) Magnetic hysteresis loops of NPLs measured with the field applied perpendicular (PER) and parallel (PAR) to the NPL's basal planes. (e) Number-weighted distribution of the hydrodynamic size of the particles suspended in RPMI-1640 medium supplemented with 10 % FBS.

spatially homogeneous or with field gradients). The size of the particles is basically limited by general therapeutic-delivery criteria, requiring the MNPs to be smaller than 200 nm to avoid the body's complement immune system from quickly removing them from the blood stream. NPs with a size of about 50 nm usually show the greatest cellular uptake [16,17]. On the other hand, the shape of NPs has a large effect on the particle's ability to travel in the blood stream [17] and it plays a key-role in transferring the produced mechanical forces to the cellular structures, e.g., lysosomal membranes. For example, the torque produced by rotational oscillations in a homogeneous AMF is only effectively transferred to the cell membrane when the magnetic particle exhibits an anisotropic shape. Due to a large contact surface, a plate-like shape is preferred for force transfer. In particular, platelet MNPs are the most effective when they exhibit an out-of-plane orientation of the magnetization [18]. Finally, the efficiency of the mechanical force's transfer will depend on the strength of the interactions between the MNPs and the cell membrane, where the MNP must be firmly "attached" to the membrane for an efficient transfer [19].

Various approaches have been proposed for the magneto-mechanical destruction of different types of cancer cells. Diverse MNPs (different size, shape, magnetic properties, surface functionalization, and the state of agglomeration) were actuated with AMFs having various characteristics. However, the diversity of magneto-mechanical approaches makes generalization of the results rather complex. Nevertheless, in general, the *in vitro* tests consistently showed a significant decrease in the cell viability, whereas the *in vivo* tests showed a significant decrease in tumour volume [5]. The effect of the MMA was ascribed to a range of different biological mechanisms at the cellular level. Larger anisotropic magnetic microparticles generally damage the plasma membrane of cells when actuated with an AMF. Notably, 1-D microparticles (e.g., spindle-like particles, nanowires) caused membrane rupture inducing necrosis [20,21], whereas programmed cell death (apoptosis) was reported for 2-D microparticles, such as lithographically fabricated, ferromagnetic microdiscs [22]. Smaller MNPs usually internalize into cells through endocytosis, eventually accumulating in the lysosomes. The decrease in cell viability was most frequently ascribed to lysosome membrane damage causing the extravasation of lysosomal contents into the cytoplasm [21,23–40]. However, in some cases a reduction in cell viability was observed even though lysosomal disruption could not be detected. The effect of MMA was thereby ascribed to a cytoskeletal disruption in the vicinity of MNP-containing lysosomes [37]. Mechanically stimulated changes in the mitochondria [39,40] and in the cellular-membrane ion metabolism [21] were also proposed as a possible mechanism leading to the apoptosis of cancer cells.

However, it is important to emphasize that it is frequently difficult to avoid any agglomeration when the NPs are introduced into a biological fluid with increased ionic strength. In addition, under an applied magnetic field the MNPs will tend to assemble into larger structures due to the magnetostatic interactions [41]. For example, under a static field they will associate into elongated, chain-like agglomerates, whereas under a rotating magnetic field they can assemble into various patterns, also referred to as swarms [23,42]. This agglomeration will strongly affect the MMA, since the collective energy transfer of many interacting MNPs in the assembly will greatly increase the force delivered during the MMA, when compared to the force of the individual, actuated MNPs. Thus, even ultra-small superparamagnetic NPs actuated with a moderate, low-frequency, rotating magnetic field can effectively destroy cancer cells when they are associated into larger assemblies inside the cells [31]. However, for an association into assemblies, NPs have to be internalized into the cells at a very high concentration. Although sufficient concentrations of MNPs can be internalized into the cells *in vitro* [31], it is questionable whether a comparably large amount of MNPs can be delivered into tumour cells in clinical praxis *in vivo*. The analysis of Wilhelm et al. [17] showed that less than 1 % of NPs will penetrate the targeted tumour after intravenous administration. Thus, it would be desirable to develop treatments that were efficient even with very low nanoparticle concentrations.

Here, we show that ferrimagnetic (permanently magnetic) hexaferrite nanoplatelets (NPLs), approximately 50 nm wide and 3 nm thick, with out-of-plane magnetization do not agglomerate inside the cells even when exposed to an AMF. Moreover, under the AMF the NPLs rotate efficiently using rather low fields even at relatively high viscosities. These characteristics lead to a very efficient reduction in the cell viability under MMA, even when using a very small number of internalized NPLs.

2. Results and discussion

2.1. Properties of nanoplatelets

The NPLs had a hexagonal shape (Fig. 1(b)). Their hexaferrite core was 52 ± 12 nm wide, whereas their thickness was defined by their unique structure at 3.0 nm, with only a minor proportion of 4.2-nm-thick NPLs [43]. The as-synthesized NPLs exhibited a saturation magnetization (M_S) of 40 Am^2/kg. The hexaferrite cores were coated with an approximately 2-nm-thick, uniform silica layer (Fig. 1(c), which was sufficient to reduce the dipolar interactions [44]). Thus, for the silica-coated NPLs, the thickness ranged from 7 to 10 nm. The NPLs exhibited very anisotropic magnetic properties. A broad, rectangular magnetic hysteresis loop (H_C = 150 kA/m) was measured when the magnetic field was applied perpendicular to the platelets and a tilted, much narrower, loop when the field was applied parallel to the platelets (Fig. 1(d)), thus confirming the out-of-plane orientation of the NPL's magnetic moment. The saturation magnetization, M_S, for the silica-coated and dextran-grafted NPLs reached 29 Am^2/kg.

Even through the NPLs exhibit permanent magnetic moments at room temperature (in contrast to the commonly used superparamagnetic NPs), the silica-coated and dextran-grafted NPLs formed colloidally stable suspensions in water, buffers and culture media. The zeta-potential of these NPLs suspended in water at neutral pH was modest, around −10 mV, suggesting that the steric repulsive forces play an important role in preventing the agglomeration. The zeta-potential also remained negative when the NPLs were suspended in the biological fluids, but the absolute value decreased, being between −3 mV and −7 mV for the buffers and culture media, respectively. A visual assessment of the suspensions over a longer period showed no sedimentation in any of the fluids. DLS measurements of the water suspensions of NPLs at neutral pH showed the hydrodynamic size of the particles ranged from 60 nm to 110 nm. When the NPLs were suspended in the buffers and different culture media the hydrodynamic size distribution changed to some extent; however, the hydrodynamic size remained below 100 nm (see Fig. 1(e) for the DLS of the NPLs in RPMI-1640 medium supplemented with 10 % FBS). These results indicate that the NPLs do not aggregate in any of the three studied media. A detailed DLS analysis of the NPLs suspended in different biological media can be found in [45].

2.2. Interaction of the nanoplatelets with an alternating magnetic field

The rotational dynamics of the NPLs exposed to an AMF was optically monitored by measuring the fluctuations induced by the AMF in the intensity of a laser-light beam transmitted through the suspension. In the absence of a magnetic field (random orientation of the NPLs), the NPLs showed an increased absorption towards short wavelengths (Fig. 2(a)). When a static magnetic field $\boldsymbol{B} = 4.5$ mT was applied parallel to the light polarization $\boldsymbol{E}$ (the NPLs oriented perpendicular to the $\boldsymbol{B}$), the transmittance of the colloidal dispersion (50 μg NPLs/mL) increased due to the reduction in light absorption by the nanoparticles in this configuration (Fig. 2(a)). The variation of the transmittance was maximized for shorter wavelengths, and decreased towards the near infrared, in which the NPLs' absorption was drastically reduced (Fig. 2(a)).

On the other hand, when a homogeneous alternating magnetic field with a frequency ω was applied, the NPLs rotated and induced a

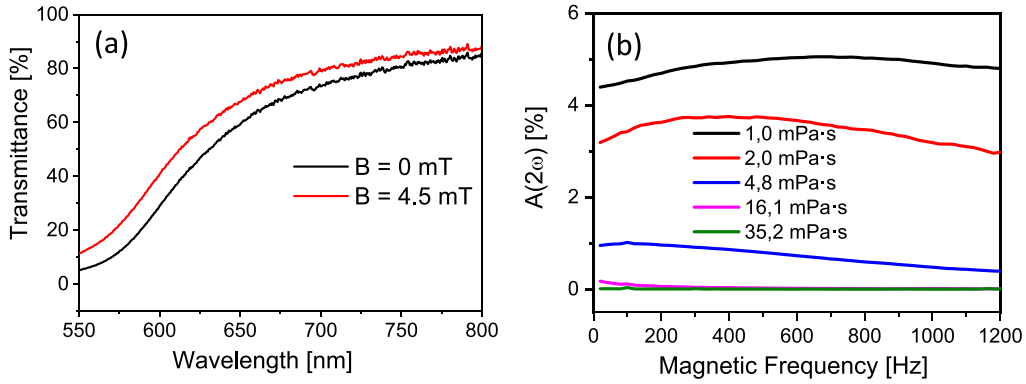

Fig. 2. Optical properties of NPL suspension at a concentration of 50 μg NPLs/mL under static and alternating magnetic fields. (a) Transmittance spectrum measured without and with an applied static magnetic field $\boldsymbol{B} = 4.5$ mT oriented parallel to the light's polarization. (b) Amplitude of transmittance variations A(2ω) (measured at 617 nm) as a function of the AMF frequency ω for NPL suspensions in liquids with different viscosities.

modulation of the transmitted light's intensity at a frequency 2ω, because the absorption of the NPLs for $+\boldsymbol{B}$ and $-\boldsymbol{B}$ is equivalent. A 617-nm laser was selected to maximize the transmittance-amplitude modulation. Fig. 2(b) shows the amplitude A(2ω) of the transmittance oscillation as a function of the magnetic field frequency ($\boldsymbol{B} = 6$ mT) and for different liquid viscosities (dependency of the amplitude A(2ω) on $\boldsymbol{B}$ is given in Fig. S1). The curves suggest that the NPLs suspended in water could rotate efficiently. Since the NPLs were in a viscous fluid, the viscous drag force meant that A(2ω) strongly depended on the field frequency. The amplitude reduction at low frequencies was due to the non-linear response of the NPLs and the generation of higher-order harmonics (A(4ω), A(6ω), …). This non-linear response was induced because the NPLs at low frequencies quickly aligned perpendicular to the field and then stayed aligned until the field changed its sign and then it quickly flipped their orientation. As a result, the transmitted intensity was not sinusoidal and higher-order harmonics appeared.

For higher frequencies, the amplitude started to decrease due to the viscous damping, thus hampering the flipping process and the following of the magnetic field. At even higher frequencies the rotational motion, i.e., the complete flip of the NPL with the alternating field changed to a vibrational motion. The most transfer of magnetic energy to mechanical energy can therefore be expected for the largest optical effect, i.e., at the frequency of the maximum A(2ω). At $\boldsymbol{B} = 6$ mT in water (viscosity 1 mPa·s) A(2ω) reached its maximum at a frequency around 600 Hz. However, the frequency of the maximum A(2ω) decreased with the increasing viscosity of the suspension medium (Fig. 2(b)), which was varied by changing the composition of the water/glycol suspension medium. Notably, this effect is relevant because the NPLs up-taken by the cells will experience an effective viscosity of the intracellular medium that is higher than that in water. The viscosity of the cytoplasm is cell-specific, spatially heterogeneous and scale dependent, i.e., objects of different sizes can experience different viscosities. The cytoplasm behaves as a liquid for smaller NPs and as a physical gel for larger particles [46]. For example, in HeLa cells NPs smaller than approximately 86 nm experience a viscosity of ≈2.0 mPa s [47]. However, the movement of NPs can also be influenced by interactions with internal structures, such as membranes. At a viscosity of 2 mPas the A(2ω) reached a maximum at a frequency of around 200 Hz, after which it started to decrease monotonously. However, when the NPLs are inside small vesicles, the effective viscosity experienced by the NPLs might be higher. For that reason, we selected frequencies in the range 1–100 Hz for the MMA experiments.

2.3. Internalization of the nanoplatelets into cancer cells

The internalization and subcellular distribution of the NPLs in the MDA-MB-231 and HeLa cells were determined using TEM. We analysed the cells treated with the NPLs for 3 h with and without exposure to the AMF ($\boldsymbol{B} = 10$ mT, f = 10 Hz, for 1 h). A STEM analysis confirmed that the NPLs up-taken into the cells retained their original morphology and the composition of the scandium-substituted barium-hexaferrite NPLs [48] (see Fig. S2 in the Supplementary Data). The NPLs were always located in membrane-enclosed compartments of the endosomal-lysosomal system. Fig. 3 shows TEM images of the NPLs internalized into the MDA-MB-231 cells, while TEM images of the HeLa cells are shown in Fig. S3 in the Supplementary Data. The NPLs were present within early and late endosomes/multivesicular bodies and endo-/lysosomes (Fig. 3). Furthermore, the NPLs were also found in amphisomes.

Only a small proportion of the ultra-thin sections of the cells contained NPLs. For example, only 13 NPLs were found in the ultra-thin sections of 42 MDA-MB-231 cells (13 ± 7 % of MDA-MB-231 cells on ultra-thin sections contained the NPLs). Assuming that the endosomal compartments containing NPLs are homogeneously distributed throughout the cells and given that the ultra-thin slice only represents approximately one 167th of the cell volume, we estimated that each MDA-MB-231 cell, on average, contained 52 NPLs. In the HeLa cells, 9 NPLs were found in 53 cells on ultra-thin sections (12 ± 4 % of the ultra-thin sections of the HeLa cells contained NPLs), which led us to estimate approximately 28 NPLs per HeLa cell. Assuming a homogeneous distribution of the NPLs and the size of the endosomal compartments (the size of endosomal compartments was measured from the TEM images to be 866 nm and 384 nm for the MDA-MB-231 and HeLa cells, respectively), we can roughly estimate that the individual endo/lysosomes contained up to 20 NPLs. Importantly, the NPLs within an individual compartment were never in direct contact (Fig. 3). Agglomerates of NPLs were never observed.

Notably, even though a small proportion of NPLs was present in the form of small groups containing several NPLs, the individual NPLs were never in close contact. Moreover, the random mutual orientation of the NPLs within a group excludes the influence of magnetic dipolar interactions on the group's formation. Namely, the magnetic interactions between permanently magnetic NPLs with the magnetic moments oriented perpendicular to the platelet plane would result in their assembly into columnar aggregates, where the NPLs are stacked in contact with the large platelet faces [49,50]. Such columnar aggregates have never been observed inside the cells, not even after the cells were exposed to the AMF. Based on these results we can conclude, with high confidence, that the NPLs behave as non-interacting particles during the exposure to an AMF, i.e., individual NPLs tend to rotate in the AMF independently and not collectively as agglomerates.

Additionally, it is important to emphasize that the inspection of the cells that were treated with the NPLs and exposed to the AMF did not reveal any changes to the structure of the cell.

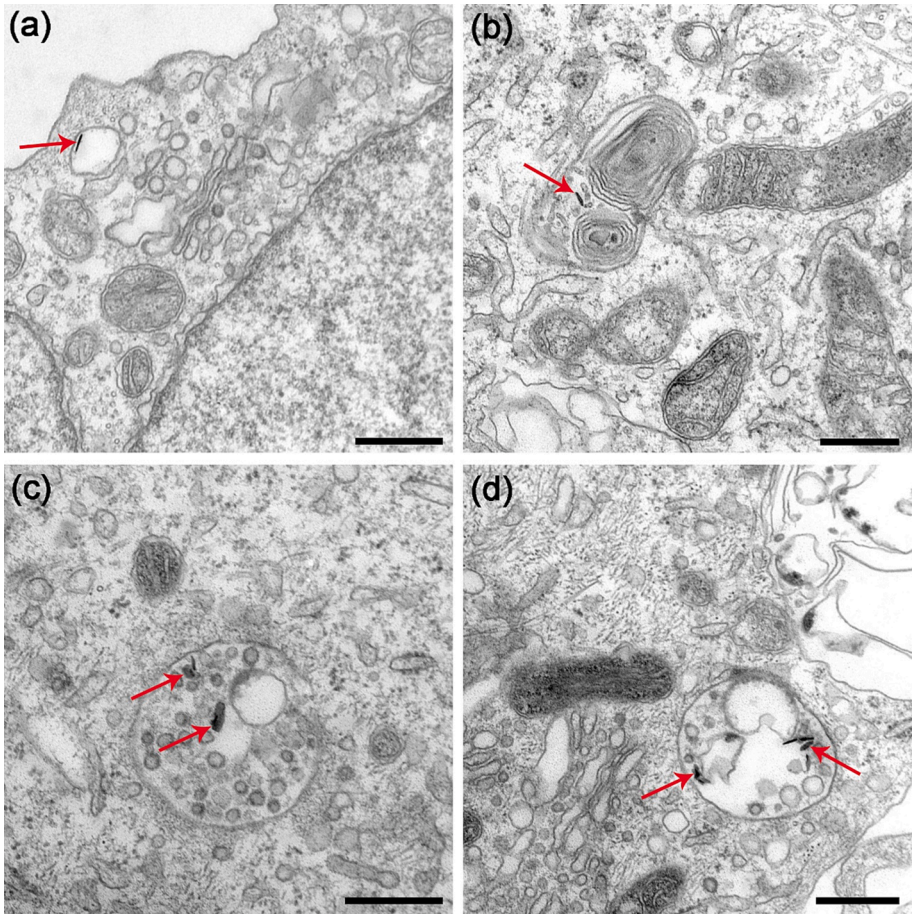

Fig. 3. TEM micrographs of MDA-MB-231 breast-cancer cells after 3 h of incubation with NPLs. NPLs (red arrows) are seen internalized in the membrane-enclosed compartments, indicating the different endolysosomal compartments (a–d). In b) the NLP is seen in amphisome. Scale bars are 400 nm. (For interpretation of the references to colour in this figure legend, the reader is referred to the web version of this article.)

2.4. Effect of nanoplatelets on the cancer-cell viability when exposed to an alternating magnetic field

To find out whether MMA can reduce the viability of cancer cells treated with NPLs, we first treated MDA-MB-231 breast-cancer cells with NPLs in the presence or absence of an AMF of $\boldsymbol{B} = 10$ mT at different frequencies. Because cancer cells are often exposed to nutrient stress in their micro-environment, we also studied whether their sensitivity to NPL/AMF treatments might differ in nutrient-replete and in serum-starved conditions. We found that treating highly tumourigenic and metastatic MDA-MB-231 breast-cancer cells with NPLs in the absence of an AMF does not affect their viability (Fig. 4). On the other hand, exposing the NPL-treated cancer cells to the AMF did compromise their viability. This effect was most significant when amino acid- and serum-starved cancer cells were treated with an AMF of higher frequencies, i.e., 10 Hz and 100 Hz (Fig. 4). This suggests that nutrient deficiency sensitizes the breast-cancer cells to magneto-mechanical actuation. Consequently, whereas NPL treatments alone did not affect the growth of the MDA-MB-231 breast-cancer cells, cell viability was significantly compromised upon exposure of the NPL-treated cells to an AMF.

To further corroborate our findings, we compared the sensitivities of two different cancer-cell lines, grown in either nutrient-rich or

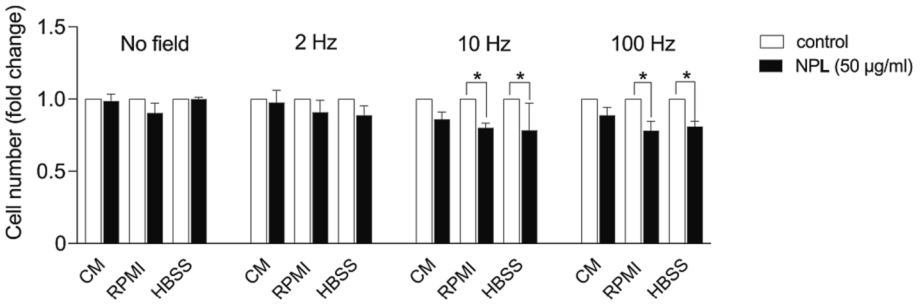

Fig. 4. MDA-MB-231 cells were grown in nutrient-replete (CM, complete media) and starvation conditions (RPMI, "mild" starvation in serum-free conditions; HBSS, "severe" starvation in the absence of amino acids and serum). Cells were treated with 50 µg/ml of NPLs for 3 h, exposed to AMF of $B = 10$ mT and $f = 2$ Hz, 10 Hz or 100 Hz, for 1 h and left to recover for 24 h. Viable cells were counted using the Scepter™ 2.0 Cell Counter. Cell numbers in each growth condition were normalized to control, i.e., untreated, cells. Values on the graphs are presented as means ± SEM of three independent experiments and results that are statistically significant are indicated (*, $P < 0.05$; **, $P < 0.01$; ***, $P < 0.001$; multiple unpaired t-tests).

starvation conditions, to treatments with different concentrations of NPLs. We found that treating aggressive MDA-MB-231 breast-cancer cells with 25 μg/ml of the NPLs and exposing them to an AMF of $\boldsymbol{B} = 10$ mT reduced the cell viability, already at the lowest frequency of 2 Hz, and particularly in starvation conditions (Fig. 5 (a)). In contrast, HeLa cervical cancer cells were found to be less sensitive to magneto-mechanical actuation treatments with the NPLs (Fig. 5(b)), although the effect of the MMA was stronger in starvation conditions. Taken together, we found that the growth of the two cancer-cell lines, which have different tissue origins, oncogenic alterations, growth characteristics and tumourigenic properties, was compromised upon magneto-mechanical actuation treatments with the NPLs.

3. Discussion

In contrast to many studies where the effect of MMA on cells was clearly associated with a collective energy transfer of many agglomerated MNPs [8,23,28–33] or using larger, lithographed particles [22], we demonstrated a significant decrease in the cell viability upon MMA using dispersed, non-interacting nanoparticles. Instead of commonly used, small, superparamagnetic NPs with an isotropic shape (with sizes typically below 15 nm), we applied permanently magnetic, barium-hexaferrite nanoplatelets (~50 nm wide and 3 nm thick) with a perpendicular orientation of the magnetic moments [45,48]. Moreover, the NPLs actuated with a low-frequency (2–100 Hz) AMF with a relatively low amplitude (10 mT) reduced the cancer-cell number and viability, even though they were internalized into the cells in relatively very low concentrations (less than one hundred NPLs per cell). Usually, several NPLs (up to 18 NPLs) were situated in individual endosomal-lysosomal compartments. The individual NPLs inside the compartments were never in close contact or mutually oriented in a way suggesting that they were magnetically interacting with each other. In our particular case, the weak uptake of the NPLs by the cells *in vitro* is most probably associated with the very good colloidal stability of the dextran-grafted NPLs in the cell medium. As the NPLs do not sediment on exposed cells, only a small proportion of the NPLs comes into the contact with the plasma membranes to have a chance of being taken up. Nevertheless, the demonstrated effect of the MMA, mediated even by a low concentration of the internalized NPLs, is important for further practical applications. Namely, the translation to clinical use is faced with various difficulties, including inefficient internalization into tumour cells [16,17]. It is difficult to see that the MNPs will internalize into the cancer cells in high enough concentrations to enable their aggregation (swarming) under the influence of an applied magnetic field in clinical conditions. In fact, the strong magnetic character of the particles (in contrast to the weak response of superparamagnetic nanoparticles) will probably help their internalization into tumours through magnetic targeting [3].

The effect of MMA mediated with the non-interacting NPLs was demonstrated on two different cancer-cell lines and under different cell-culture conditions, which are rarely studied, even though it may affect the outcome of the MMA. It is not clear if the culturing conditions affect the cytotoxicity generated by MMA directly or if they only increase the sensitivity of the cancer cells to the MMA. Importantly, the non-actuated NPLs did not show any cytotoxic effects when tested in different culture media. Accordingly, we did not observe any effects of the NPLs on the MDA-MB-231 cell number in the absence of an AMF, regardless of their growth in media containing varying levels of nutrients and growth factors. This demonstrates that their effect on the cancer-cell viability depends solely on the MMA. Indeed, aggressive cancer cells driven by the Ras oncogene, such as MDA-MB-231 cells, have enhanced capacities to adapt to various stress conditions induced by nutrient or oxygen deficiencies [51,52]. These cancer cells can modulate their metabolic and signalling pathways to match the growth rates with nutrient availability. For example, the absence of serum, which is the primary source of lipids during growth in nutrient-rich media, activates the metabolic pathways in the MDA-MB-231 cells that convert glucose to lipids (de novo lipogenesis) to compensate for the lack of lipids and maintain membrane homeostasis and cell survival [53,54]. Serum-free cell-culture media still contain enough glucose, amino acids and vitamins to support lipogenesis and cancer-cell survival under these conditions. During severe nutrient deficiency, which can be mimicked *in vitro* using a buffer containing minimal levels of glucose, such as HBSS, aggressive cancer cells also employ opportunistic modes for the acquisition of extracellular material through macropinocytosis, thereby engulfing the extracellular proteins, apoptotic bodies and even living cells [55]. Thus, nutrient availability and the metabolic status of cancer cells can have a strong impact on their propensity to uptake extracellular material. In this study, the effects of NPLs on cancer cells were examined in three different media that induce varying levels of stress and modulate the essential metabolic and nutrient-acquisition pathways. Although the effects of MM-actuated NPLs on cell viability were slightly more pronounced in starvation media, the presence or absence of the serum did not alter these effects significantly. Moreover, serum-starved and severely starved MDA-MB-231 cells had comparable sensitivities to the MM-actuated NPLs. In addition, HeLa cervical cancer cells, which differ from the MDA-MB-231 cells in the underlying oncogenic drivers and metabolic hallmarks, were also sensitive to the MM-actuated NPLs. Interestingly, the HeLa cells seem to be more sensitive to the starvation conditions than the MDA-MB-231 cells. The TEM analysis suggested that the NPLs were internalized to a similar extent in the various growth conditions and in both cell lines, irrespective of their intrinsic differences in the stress-induced metabolic and nutrient-acquisition mechanisms. This indicates that the observed heightened sensitivity of starving cancer cells to MM-actuated NPLs is not attributable to varying efficiencies in NPL internalization. Instead, specific alterations in cancer-

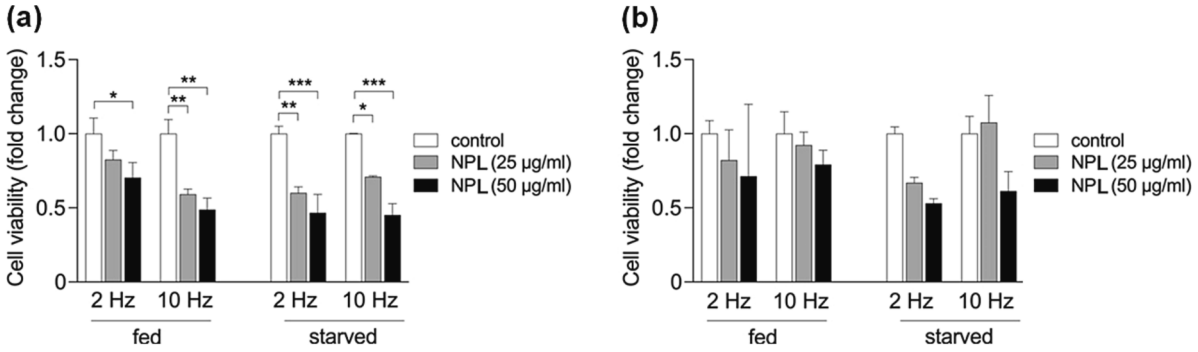

Fig. 5. MDA-MB-231 breast-cancer (a) and Hela cervical cancer (b) cells were treated with 25 or 50 μg/ml of NPLs for 24 h followed by exposure to AMF, $\boldsymbol{B} = 10$ mT, f = 2 or 10 Hz for 1 h. After 24 h, cell viability was determined by Presto Blue staining and fluorescence measurements. Fed cells were grown in a culture medium, whereas starved cells were in HBSS. Values on the graphs are presented as means ± SEM of at least two independent experiments and results that are statistically significant are indicated (*, $P < 0.05$; **, $P < 0.01$; ***, $P < 0.001$; two-way ANOVA with Tukey's adjustment).

cell metabolism and function induced by starvation [47] appear to render them more responsive to the effects of MMA mediated by internalized NPLs. Therefore, it is plausible that nutrient deficiency, frequently encountered by cancer cells during tumour initiation, progression, and metastasis in poorly vascularized microenvironmental regions, or pharmacological treatments targeting cancer metabolism that induce starvation-like states in cancer cells, could potentially enhance the efficacy of a magnetic cancer treatment.

Since the effect of the MMA was related to the low concentration of NPLs present in the cells, we were not able to identify any specific cellular mechanism as being responsible for the observed decrease in the cell viability. However, our tests on giant unilamellar vesicles, which represented a simple model for the cell membrane, showed that the hexaferrite NPLs could exert large mechanical forces to disrupt the phospholipid bilayer membranes when actuated with a homogeneous uniaxial AMF (3–100 Hz) at relatively modest amplitudes, below 10 mT. In contrast to previous theoretical considerations suggesting that the membrane ruptures are due to the local action of an assembly of several NPLs [19], we demonstrated that non-agglomerated NPLs can efficiently compromise cell viability.

4. Conclusions

A study of the viability of cancer cells using magneto-mechanical actuation (MMA) mediated by non-agglomerated, permanently magnetic ($M_S \sim 40$ Am^2/kg), silica-coated barium-hexaferrite nanoplatelets (NPLs) was presented in cells at very low concentrations (ca. 50 NPLs per cell), located within the membrane-enclosed compartments of an endosomal-lysosomal system (1–5 NPLs per compartment). Even at low concentrations of the non-interacting NPLs the MMA (2–100 Hz, 10 mT) effectively reduced the cell viability in two cancer-cell lines (MDA-MB-231 human breast adenocarcinoma cells and HeLa cervical adenocarcinoma cells). Notably, the impact of the MMA was greater in nutrient-deprived cancer cells, and this sensitization was not dependent on variations in the NPL internalization efficiencies in nutrient-rich and starvation conditions. We speculate that specific metabolic and functional changes induced by nutrient deficiency in cancer cells underlay this increased sensitivity, but the mechanisms remain to be investigated. Nonetheless, our observations suggest a potential for enhancing magnetic cancer therapy by combining drugs that specifically target cancer-nutrient sensing and metabolic pathways in cancer cells alongside MMA mediated by NPLs. Thus, the synergistic effect of starvation and MMA presents a promising avenue for further research and potential treatment options for cancer. To conclude, our results pave the way for efficient magneto-mechanical tumour eradication *in vivo*, where the internalization of large numbers of nanoparticles into cancer cells cannot be expected.

5. Methods

5.1. Preparation of nanoplatelet suspensions

Colloidally stable, aqueous suspensions of NPLs were prepared as reported [45]. First, the hydrothermally synthesized, scandium-substituted, barium-hexaferrite NPLs [56] were dispersed in water using electrostatic stabilization of the suspension with citric acid. Then, the NPLs were coated with a thin layer of silica by hydrolysis and the polycondensation of tetraethyl orthosilicate (TEOS) in suspension [57]. For tracking the NPLs with methods based on fluorescence microscopy, a fluorescent dye called rhodamine B was incorporated into the silica deposited on some of the NPLs. Finally, dextran molecules (MW ca. 20,000 Da) were covalently grafted onto the surfaces of the silica-coated NPLs using the 3-glycidyloxypropyl-trimethoxysilane linker to enable their colloidal stability in cell media. The details of the suspension-preparation procedures are given in the Supplementary Data.

5.2. Characterization of nanoplatelet suspensions

The NPLs were characterized using a transmission electron microscope (TEM Jeol 2010F) and a probe spherical-aberration corrected (C_S) scanning-transmission electron microscope (STEM Jeol ARM 200CF). The magnetic properties of the NPLs were measured at room temperature with a vibrating-sample magnetometer (VSM, Lakeshore 7407) after they were aligned in the magnetic field. The NPLs hydrophobized by the adsorption of ricinoleic acid onto their surfaces were dispersed in a hot liquid wax, aligned with the homogeneous magnetic field (H = 1000 kA/m) and then the wax was solidified by cooling to retain the texture (see the Supplementary Data for details). The zeta-potential and the hydrodynamic size of the NPLs in suspensions were measured with ZetaPALS (Brookhaven Instruments Corporation) and Analysette 12 DynaSizer (Fritsch) instruments, respectively, based on dynamic light scattering (DLS).

The rotational dynamics of the dispersed NPLs under a homogeneous AMF were followed by measuring the fluctuations in the intensity of a laser beam transmitted through the suspension. The rotational oscillations of the NPLs under the AMF result in a strong magneto-chromic effect, i.e., an intense modulation of the light transmitted through the suspension of NPLs [58,59]. The light-intensity fluctuations using a 617-nm-wavelength laser were measured as a function of the AMF frequency in liquid media with varying viscosity. The viscosity of the medium was varied by mixing water and glycol in different proportions.

5.3. Materials, cell culture and treatments

Human breast adenocarcinoma cells (MDA-MB-231), HeLa cervical adenocarcinoma cells and a RPMI-1640 culture medium were obtained from ATCC (USA), foetal bovine serum (FBS), high glucose DMEM media supplemented with GlutaMAX, Dulbecco's phosphate-buffered saline (DPBS), Hanks' balanced salt solution (HBSS) and TrypLE Select from Gibco (USA). Propidium iodide was from Life Technologies (USA), Presto Blue Cell Viability Reagent from Invitrogen (USA), and fatty acid-free bovine serum albumin (BSA) (cat. No. A8806) from Sigma-Aldrich (USA).

MDA-MB-231 cells were cultured in RPMI-1640 and HeLa cells in DMEM media, both supplemented with 10 % FBS (hereafter termed "complete" media). Adherent cells were detached using TrypLE Select. Unless otherwise indicated, MDA-MB-231 and HeLa cells were seeded in 24-well plates at a density of 1.6×10^4 cells/cm^2 and 0.8×10^4 cells/cm^2, respectively, and grown for 24 h in complete medium. After 24 h, the cells were washed twice with DPBS, placed in starvation media (either serum-free RPMI-1640 medium containing 0.02 % BSA or serum- and amino acid-free HBSS buffer containing 0.02 % BSA) and treated with 50 μg/ml of the NPLs for 3 or 24 h. After the treatment, the cells were exposed to the AMF at room temperature and left for an additional 24 h at 37 °C and 5 % CO_2 to recover.

5.4. TEM analysis of cells

MDA-MB-231 cells at 4.3×10^4 cells/cm^2 and HeLa cells at 2.2×10^4 cells/cm^2 were grown on 35-mm plates in complete medium. After 24 h the cells were treated with 50 μg/ml of the NPLs in complete medium for 3 h. Then, the cells were exposed to the AMF ($f = 10$ Hz, $B = 10$ mT), for 1 h at room temperature. After 24 h, the cells were washed with DPBS and fixated in a mixture of 3 % glutaraldehyde (v/v) and paraformaldehyde (w/v) in 0.1-M cacodylate buffer, pH 7.4 at 4 °C for 3 h, followed by overnight rinsing in 0.33-M sucrose at 4 °C. The samples were then post-fixed in 1 % (w/v) osmium tetroxide for 1 h at room temperature, rinsed in distilled water, and incubated in 2 % uranyl acetate for 1 h at room temperature and rinsed again in distilled water. Samples were then dehydrated in a graded series of ethanol (50, 70, 90 %) for 15 min each and 100 % ethanol for 30 min, twice. Dehydrated samples were then embedded in Epon by infiltration. The

polymerisation of Epon was performed over the next 5 days with a gradual temperature increase (35 °C, 45 °C, 60 °C, 70 °C and 80 °C) every 24 h. The untreated cells (control), the cells treated with the NPLs, and the cells treated with the NPLs and exposed to the AMF were prepared in parallel. Next, 60-nm ultra-thin sections were prepared with Ultramicrotome (Leica EM UC6) and collected on formvar-coated copper grids and counterstained with uranyl acetate and lead citrate. The samples were observed on a Philips CM 100 electron microscope operating at an accelerating voltage of 80 kV.

To estimate the internalization of the NPLs in MDA-MB-231 and HeLa cells treated with NPLs, five 60-nm ultra-thin sections were systematically prepared from each sample as described in [60]. Each sample was sectioned with the ultra-microtome at 100 μm intervals (60-nm ultra-thin sections were made), so that each individual cell was sectioned only once. For the TEM analysis, high-quality micrographs were independently assessed by two of the authors. The assessors had no prior knowledge of the cell type or how the cells were treated. TEM micrographs at 6600–11,500× magnification were used to examine each cell on the sections for internalized NPLs. Only cells with visible nuclei were analysed. Notably, NPLs were always found in membrane-enclosed compartments. The percentages of MDA-MB-231 and HeLa cells containing NPLs in the endosomal compartment were determined by analysing cells on five ultra-thin sections (average 9 cells per section). We analysed all the cells on the ultra-thin sections and classified them as positive or negative for NPLs, assuming that the endosomal compartments containing NPLs were homogeneously distributed throughout the cells. Subsequently, the number of NPLs per cross-section of NPL-positive endosomal compartments of MDA-MB-231 and HeLa cells was counted manually.

5.5. Cell-viability assay

MDA-MB-231 cells were seeded on 96-well culture plates at 2.1×10^4 cells/cm^2 and HeLa cells at 1.0×10^4 cells/cm^2. After 24 h the cells were washed twice with DPBS and incubated for the next 24 h in either complete medium or in serum-free starvation medium (RPMI-1640 containing 0.02 % BSA for MDA-MB-231 cells and DMEM containing 0.02 % BSA for HeLa cells). Cells were then treated with 25 or 50 μg/ml of NPLs for 3 h followed by an exposure to an AMF of $f = 2$ Hz, $f = 10$ Hz or $f = 100$ Hz and $\boldsymbol{B}$ of 10 mT for 1 h at room temperature, and left in the incubator (37 °C, 5 % CO_2) for an additional 24 h to recover. Cell viability was determined using the PrestoBlue Cell Viability Reagent (Invitrogen, USA) according to the manufacturer's instructions and a Tecan Infinite M1000 microplate reader (Tecan, Austria).

5.6. Cell counting

The MDA-MB-231 cells were seeded on 12-well culture plates at 1.7×10^4 cells/cm^2 in complete medium. After 24 h the cells were washed twice with DPBS, the media replaced with fresh complete or starvation media (either serum-free RPMI-1640 medium containing 0.02 % BSA or serum and amino acid-free HBSS containing 0.02 % BSA) and the cells treated with 50 μg/ml NPLs for 24 h. The cells were then exposed to an AMF of $f = 2$ Hz, $f = 10$ Hz or $f = 100$ Hz and B of 10 mT for 1 h at room temperature and left for an additional 24 h at 37 °C and 5 % CO_2 to recover. For viable-cell counting, the cells were detached, resuspended in DPBS and 50 μl of the cell suspension was drawn through the cell-sensing tip of a Scepter™ 2.0 Cell Counter (Millipore, USA) and analysed using the Scepter 2.0 software.

5.7. Statistical analysis

Statistical analyses were performed using GraphPad Prism 9.0.2 (GraphPad software, USA). Unless otherwise indicated, data are presented as means ± SEM of at least three independent experiments. Statistical significance was determined using Student's *t*-test, one-way or two-way ANOVA followed by Bonferroni or Tukey's post-hoc tests. P values lower than 0.05 were considered statistically significant.

CRediT authorship contribution statement

Tanja Goršak: Conceptualization, Formal analysis, Investigation, Methodology, Visualization. **Eva Jarc Jovičić:** Formal analysis, Funding acquisition, Investigation, Methodology, Validation, Visualization, Writing – review & editing. **Larisa Tratnjek:** Formal analysis, Investigation, Methodology, Visualization. **Igor Križaj:** Funding acquisition, Resources. **Borja Sepulveda:** Conceptualization, Formal analysis, Investigation, Methodology, Visualization, Writing – original draft. **Josep Nogues:** Conceptualization, Formal analysis, Investigation, Visualization, Writing – original draft. **Mateja Erdani Kreft:** Formal analysis, Funding acquisition, Investigation, Methodology, Supervision, Validation, Visualization, Writing – review & editing. **Toni Petan:** . **Slavko Kralj:** Conceptualization, Formal analysis, Investigation, Supervision, Writing – review & editing. **Darko Makovec:** Conceptualization, Data curation, Formal analysis, Funding acquisition, Investigation, Methodology, Resources, Supervision, Validation, Visualization, Writing – original draft, Writing – review & editing.

Declaration of competing interest

The authors declare that they have no known competing financial interests or personal relationships that could have appeared to influence the work reported in this paper.

Data availability

Data will be made available on request.

Acknowledgments

The support of the Slovenian Research and Innovation Agency (ARIS) within the Project L2-3040, P2-0089, P1-0207 and P3-0108 is acknowledged. BS and JN acknowledge the support of the PID2019-106229RB-I00 grant by MCIN/AEI/10.13039/ and the 2021-SGR-00651 project by the Generalitat de Catalunya. ICN2 is funded by the CERCA programme/Generalitat de Catalunya. The ICN2 is supported by the CEX2021-001214-S grant funded by MCIN/AEI/10.13039/501100011033.

Appendix A. Supplementary material

Supplementary data to this article; synthesis and characterization protocols, rotational dynamics of the nanoplatelets, and TEM / STEM analyses of nanoplatelets internalized into the cells can be found online at https://doi.org/10.1016/j.jcis.2023.12.019.

References

[1] T.K. Thanh Nguyen, Magnetic Nanoparticles from Fabrication to Clinical Applications, CRC Press, Boca Raton, USA, 2012.
[2] S. Kralj, T. Potrc, P. Kocbek, S. Marchesan, D. Makovec, Design and fabrication of magnetically responsive nanocarriers for drug delivery, Curr. Med. Chem. 24 (2017) 454–469.
[3] A. Fluksman, A. Lafuente, Z. Li, J. Sort, S. Lope-Piedrafita, M.J. Esplandiu, J. Nogues, A.G. Roca, O. Benny, B. Sepulveda, Efficient tumor eradication at ultralow drug concentration via externally controlled and boosted metallic iron magnetoplasmonic nanocapsules, ACS Nano 17 (2023) 1946–1958.
[4] C. Wu, Y. Shen, M. Chen, K. Wang, Y. Li, Y. Cheng, Recent advances in magnetic-nanomaterial-based mechanotransduction for cell fate regulation, Adv. Mater. 30 (2018), 1705673.
[5] C. Naud, C. Thebault, M. Carriere, Y. Hou, R. Morel, F. Berger, B. Dieny, H. Joisten, Cancer treatment by magneto-mechanical effect of particles, a review, Nanoscale Adv. 2 (2020) 3632–3655.
[6] Y.I. Golovin, S.L. Gribanovsky, D.Y. Golovin, N.L. Klyachko, A.G. Majouga, A. M. Master, M. Sokolsky, A.V. Kabanov, Towards nanomedicines of the future:

Remote magneto-mechanical actuation of nanomedicines by alternating magnetic fields, J. Control. Release 219 (2015) 43–60.
[7] Y.I. Golovin, A.O. Zhigachev, M.V. Efremova, A.G. Majouga, A.V. Kabanov, N. L. Klyachko, Ways and methods for controlling biomolecular structures using magnetic nanoparticles activated by an alternating magnetic field, Nanotechnol. Russ. 13 (2018) 295–307.
[8] P.N. Semina, I.L. Isaev, S.V. Komogortsev, A.B. Klyuchantsev, A.S. Kostyukov, A. V. Blagodatova, D.E. Khrennikov, A.S. Kichkailo, T.N. Zamay, I.N. Lapin, A. E. Sokolov, S.P. Polyutov, S.V. Karpov, Towards understanding the triggering of the malignant cell death in high-efficiency magneto-mechanical anticancer therapy, J. Phys. D: Appl. Phys. 56 (2023), 065401-1–065401-19.
[9] K. Maier-Hauff, F. Ulrich, D. Nestler, H. Niehoff, P. Wust, B. Thiesen, H. Orawa, V. Budach, A. Jordan, Efficacy and safety of intratumoral thermotherapy using magnetic iron-oxide nanoparticles combined with external beam radiotherapy on patients with recurrent glioblastoma multiforme, J. Neurooncol. 103 (2011) 317–324.
[10] R. Weissleder, M. Nahrendorf, M.J. Pittet, Imaging macrophages with nanoparticles, Nat. Mater. 13 (2014) 125–138.
[11] B. Gleich, J. Weizenecker, Tomographic imaging using the nonlinear response of magnetic particles, Nature 435 (2005) 1214–1217.
[12] E.Y. Yu, M. Bishop, B. Zheng, R.M. Ferguson, A.P. Khandhar, S.J. Kemp, K. M. Krishnan, P.W. Goodwill, S.M. Conolly, Magnetic particle imaging: a novel in vivo imaging platform for cancer detection, Nano Lett. 17 (2017) 1648–1654.
[13] A.K. Hauser, R.J. Wydra, N.A. Stocke, K.W. Anderson, J.Z. Hilt, Magnetic nanoparticles and nanocomposites for remote controlled therapies, J. Control. Release 219 (2015) 76–94.
[14] S. Nappini, F. Baldelli Bombelli, M. Bonini, B. Norden, P. Baglioni, Magnetoliposomes for controlled drug release in the presence of low frequency magnetic field, Soft Matter 6 (2010) 154–162.
[15] J. Tumpane, N. Karousis, N. Tagmatarchis, B. Norden, Alignment of carbon nanotubes in weak magnetic fields, Angew. Chem. Int. Ed. 47 (2008) 5148–5152.
[16] N. Hoshyar, S. Gray, H. Han, G. Bao, The effect of nanoparticle size on in vivo pharmacokinetics and cellular interaction, Nanomedicine (Lond.) 11 (2016) 673–692.
[17] S. Wilhelm, A.J. Tavares, Q. Dai, S. Ohta, J. Audet, H.F. Dvorak, W.C.W. Chan, Analysis of nanoparticle delivery to tumours, Nat. Rev. Mater. 1 (2016) 1–12.
[18] R. Mansell, T. Vemulkar, D.C.M.C. Petit, Y. Cheng, J. Murphy, M.S. Lesniak, R. P. Cowburn, Magnetic particles with perpendicular anisotropy for mechanical cancer cell destruction, Sci. Rep. 7 (2017), 4257-1–4257-7.
[19] T. Goršak, M. Drab, D. Križaj, M. Jeran, J. Genova, S. Kralj, D. Lisjak, V. Kralj-Iglič, A. Iglič, D. Makovec, Magneto-mechanical actuation of barium-hexaferrite nanoplatelets for the disruption of phospholipid membranes, J. Colloid Interface Sci. 579 (2020) 508–519.
[20] M.F. Contreras, R. Sougrat, A. Zaher, T. Ravasi, J. Kosel, Non-chemotoxic induction of cancer cell death using magnetic nanowires, Int. J. Nanomed. 10 (2015) 2141–2153.
[21] B. Wang, C. Bienvenu, J. Mendez-Garza, P. Lançon, A. Madeira, P. Vierling, C. Di Giorgio, G. Bossis, Necrosis of HepG2 cancer cells induced by the vibration of magnetic particles, J. Magn. Magn. Mater. 344 (2013) 193–201.
[22] D.-H. Kim, E.A. Rozhkova, I.V. Ulasov, S.D. Bader, T. Rajh, M.S. Lesniak, V. Novosad, Biofunctionalized magnetic-vortex microdiscs for targeted cancer-cell destruction, Nat. Matter. 9 (2010) 165–171.
[23] Y. Shen, W. Zhang, G. Li, P. Ning, Z. Li, H. Chen, X. Wei, X. Pan, Y. Qin, B. He, Z. Yu, Y. Cheng, Adaptive control of nanomotor swarms for magnetic-field-programmed cancer cell destruction, ACS Nano 15 (2021) 20020–20031.
[24] Y. Cheng, M.E. Muroski, D.C. Petit, R. Mansell, T. Vemulkar, R.A. Morshed, Y. Han, I.V. Balyasnikova, C.M. Horbinski, X. Huang, L. Zhang, R.P. Cowburn, M. S. Lesniak, Rotating magnetic field induced oscillation of magnetic particles for in vivo mechanical destruction of malignant glioma, J. Control. Release 223 (2016) 75–84.
[25] M. Domenech, I. Marrero-Berrios, M. Torres-Lugo, C. Rinaldi, Lysosomal membrane permeabilization by targeted magnetic nanoparticles in alternating magnetic fields, ACS Nano 7 (2013) 5091–5101.
[26] E. Zhang, M.F. Kircher, M. Koch, L. Eliasson, S.N. Goldberg, E. Renström, Dynamic magnetic fields remote-control apoptosis via nanoparticle rotation, ACS Nano 8 (2014) 3192–3201.
[27] O. Lunov, M. Uzhytchak, B. Smolkova, M. Lunova, M. Jirsa, N.M. Dempsey, A. L. Dias, M. Bonfim, M. Hof, P. Jurkiewicz, Y. Petrenko, Š. Kubinova, A. Dejneka, Remote actuation of apoptosis in liver cancer cells via magneto-mechanical modulation of iron oxide nanoparticles, Cancers 11 (2019) 1–20.
[28] S. Hapuarachchige, Y. Kato, E.J. Ngen, B. Smith, M. Delannoy, D. Artemov, Non-temperature induced effects of magnetized iron oxide nanoparticles in alternating magnetic field in cancer cells, PLoS One 11 (2016) e0156294-1–e0156294-12.
[29] Y. Shen, C. Wu, T.Q. Uyeda, G.R. Plaza, B. Liu, Y. Han, M.C. Lesniak, Y. Cheng, Elongated nanoparticle aggregates in cancer cells for mechanical destruction with low frequency rotating magnetic field, Theranostics 7 (2017) 1735–1748.
[30] O.S. Kolovskaya, T.N. Zamay, G.S. Zamay, V.A. Babkin, E.N. Medvedeva, N. A. Neverova, A.K. Kirichenko, S.S. Zamay, I.N. Lapin, E.V. Morozov, A.E. Sokolov, A.A. Narodov, D.G. Fedorov, F.N. Tomilin, V.N. Zabluda, Y. Alekhina, K. A. Lukyanenko, Y.E. Glazyrin, V.A. Svetlichnyi, M.V. Berezovski, A.S. Kichkailo, Aptamer-conjugated superparamagnetic ferroarabinogalactan nanoparticles for targeted magnetodynamic therapy of cancer, Cancers 12 (2020), 216-1–216-17.
[31] J. Wu, P. Ning, R. Gao, Q. Feng, Y. Shen, Y. Zhang, Y. Li, C. Xu, Y. Qin, G.R. Plaza, Q. Bai, X. Fan, Z. Li, Y. Han, M.S. Lesniak, H. Fan, Y. Cheng, Programmable ROS-mediated cancer therapy via magneto-inductions, Adv. Sci. 7 (2020), 1902933-1–1902933-16.
[32] S. Lopez, N. Hallali, Y. Lalatonne, A. Hillion, J.C. Antunes, N. Serhan, P. Clerc, D. Fourmy, L. Motte, J. Carrey, V. Gigoux, Magneto-mechanical destruction of cancer associated fibroblasts using ultra-small iron oxide nanoparticles and low frequency rotating magnetic fields, Nanoscale Adv. 4 (2022) 421–436.
[33] A.S. Garanina, M.V. Efremova, A.E. Machulkin, E.V. Lyubin, N.S. Vorobyeva, O.A. Zhironkina, O.S. Strelkova, I.I. Kireev, I.B. Alieva, R.E. Uzbekov, V.N. Agafonov, I. V. Shchetinin, A.A. Fedyanin, A.S. Erofeev, P.V. Gorelkin, Y.E. Korchev, A.G. Savchenko, M.A. Abakumov, Bifunctional magnetite–gold nanoparticles for magneto-mechanical actuation and cancer cell destruction, Magnetochemistry 8 (2022) 185-1–185-18.
[34] A. Hillion, N. Hallali, P. Clerc, S. Lopez, Y. Lalatonne, C. Noûs, L. Motte, V. Gigoux, J. Carrey, Real-time observation and analysis of magnetomechanical actuation of magnetic nanoparticles in cells, Nano Lett. 22 (2022) 1986–1991.
[35] Y. Zhang, H.P. Hu, W.Q. Tang, Q. Zhang, M. Li, H.L. Jin, Z. Huang, Z. Cui, J.Y. Xu, K.P. Wang, C. Shi, A multifunctional magnetic nanosystem based on ″two strikes″ effect for synergistic anticancer therapy in triple-negative breast cancer, J. Control. Release 322 (2020) 401–415.
[36] H. Du, F. Yang, C. Yao, W. Lv, H. Peng, S.G. Stanciu, H.A. Stenmark, Y. Min Song, B. Jiang, A. Wu, "Double-punch" strategy against triple-negative breast cancer via a synergistic therapy of magneto-mechanical force enhancing NIR-II hypothermal ablation, Biomaterials 291 (2022), 121868-1–121868-12.
[37] J. Liu, W. Yang, Y. Huang, J. Liu, W. Yang, Y. Huang, J. Li, C. Zhu, G. Pu, B. Wang, X. Gui, M. Chu, Oxygen and hydrogen peroxide self-supplying magnetic nanoenzymes for cancer therapy through magneto-mechanical force, force-induced reactive oxygen species, chemodynamic effects, and cytotoxicity of Ca2+ ions, Nano Res. (2023), https://doi.org/10.1007/s12274-022-5303-5.
[38] A.M. Master, P.N. Williams, N. Pothayee, N. Pothayee, R. Zhang, H.M. Vishwasrao, Y.I. Golovin, J.S. Riffle, M. Sokolsky, A.V. Kabanov, Remote actuation of magnetic nanoparticles for cancer cell selective treatment through cytoskeletal disruption, Sci. Rep. 6 (2016), 33560-1–33560-13.
[39] M. Chen, J. Wu, P. Ning, J. Wang, Z. Ma, L. Huang, G.R. Plaza, Y. Shen, C. Xu, Y. Han, M.S. Lesniak, Z. Liu, Y. Cheng, Remote control of mechanical forces via mitochondrial-targeted magnetic nanospinners for efficient cancer treatment, Small 16 (2020), 1905424-1–1905424-14.
[40] W. Park, S.-J. Kim, P. Cheresh, J. Yun, B. Lee, D.W. Kamp, D.-H. Kim, Magneto mitochondrial dysfunction mediated cancer cell death using intracellular magnetic nano-transducers, Biomater. Sci. 9 (2021) 5497–5507.
[41] S. Odenbach, Colloidal Magnetic Fluids: Basics, Development and Application of Ferrofluids, Springer, Berlin, Heidelberg, Germany, 2009.
[42] J. Carrey, N. Hallali, Torque undergone by assemblies of single-domain magnetic nanoparticles submitted to a rotating magnetic field, Phys. Rev. B 94 (2016), 184420-1–184420-18.
[43] D. Makovec, B. Belec, T. Goršak, D. Lisjak, M. Komelj, G. Dražić, S. Gyergyek, Discrete evolution of the crystal structure during the growth of Ba-hexaferrite nanoplatelets, Nanoscale 10 (2018) 14480–14491.
[44] J.A. De Toro, M. Vasilakaki, S.S. Lee, M.S. Andersson, P.S. Normile, N. Yaacoub, P. Murray, E.H. Sánchez, P. Muñiz, D. Peddis, R. Mathieu, K. Liu, J. Geshev, K. N. Trohidou, J. Nogués, Remanence plots as a probe of spin disorder in magnetic nanoparticles, Chem. Mater. 29 (2017) 8258–8268.
[45] T. Goršak, D. Makovec, U. Javornik, B. Belec, S. Kralj, D. Lisjak, A functionalization strategy for the dispersion of permanently magnetic barium-hexaferrite nanoplatelets in complex biological media, Colloids Surf. A: Physicochem. Eng. Asp. 573 (2019) 119–127.
[46] K. Kwapiszewska, K. Szczepański, T. Kalwarczyk, B. Michalska, P. Patalas-Krawczyk, J. Szymański, T. Andryszewski, M. Iwan, J. Duszyński, R. Hołyst, Nanoscale viscosity of cytoplasm is conserved in human cell lines, J. Phys. Chem. Lett. 11 (2020) 6914–6920.
[47] T. Kalwarczyk, N. Ziebacz, A. Bielejewska, E. Zaboklicka, K. Koynov, J. Szymanski, A. Wilk, A. Patkowski, J. Gapinski, H.-J. Butt, R. Hozyst, Comparative analysis of viscosity of complex liquids and cytoplasm of mammalian cells at the nanoscale, Nano Lett. 11 (2011) 2157–2163.
[48] D. Makovec, M. Komelj, G. Dražić, B. Belec, T. Goršak, S. Gyergyek, D. Lisjak, Incorporation of Sc into the structure of barium-hexaferrite nanoplatelets and its extraordinary finite-size effect on the magnetic properties, Acta Mater. 172 (2019) 84–91.
[49] P. Hribar Boštjančič, M. Tomšič, A. Jamnik, D. Lisjak, A. Mertelj, Electrostatic interactions between barium hexaferrite nanoplatelets in alcohol suspensions, J. Phys. Chem. C 123 (2019) 23272–23279.
[50] A.A. Eliseev, L.A. Trusov, E.O. Anokhin, A.P. Chumakov, V.V. Korolev, A. E. Sleptsova, P. Boesecke, V.I. Pryakhina, V.Y. Shur, P.E. Kazin, A.A. Eliseev, Tunable order in colloids of hard magnetic hexaferrite nanoplatelets, Nano Res. 15 (2022) 898–906.
[51] N.N. Pavlova, C.B. Thompson, The emerging hallmarks of cancer metabolism, Cell Metab. 23 (2016) 27–47.
[52] J.J. Kamphorst, J.R. Cross, J. Fan, E. de Stanchina, R. Mathew, E.P. White, C. B. Thompson, J.D. Rabinowitz, Hypoxic and Ras-transformed cells support growth by scavenging unsaturated fatty acids from lysophospholipids, Proc. Natl. Acad. Sci. 110 (2013) 8882–8887.
[53] A. Pucer, V. Brglez, C. Payré, J. Pungerčar, G. Lambeau, T. Petan, Group X secreted phospholipase A2 induces lipid droplet formation and prolongs breast cancer cell survival, Mol. Cancer 12 (2013) 111.
[54] T. Petan, Lipid Droplets in Cancer, Rev. Physiol. Biochem. Pharmacol. 185 (2023) 53–86.
[55] W. Palm, C.B. Thompson, Nutrient acquisition strategies of mammalian cells, Nature 546 (2017) 234–242.

[56] D. Lisjak, M. Drofenik, Chemical substitution: an alternative strategy for controlling the particle size of barium ferrite, Cryst. Growth Des. 12 (2012) 5174–5179.
[57] S. Kralj, D. Makovec, S. Čampelj, M. Drofenik, Producing ultra-thin silica coatings on iron-oxide nanoparticles to improve their surface reactivity, J. Magn. Magn. Mater. 322 (2010) 1847–1853.
[58] A.A. Eliseev, A.A. Eliseev, L.A. Trusov, A.P. Chumakov, P. Boesecke, E.O. Anokhin, A.V. Vasiliev, A.E. Sleptsova, E.A. Gorbachev, V.V. Korolev, P.E. Kazin, Rotational dynamics of colloidal hexaferrite nanoplates, Appl. Phys. Lett. 113 (2018), 113106-1–113106-5.
[59] Z. Li, A. Lopez-Ortega, A. Aranda-Ramos, J.L. Tajada, J. Sort, C. Nogues, P. Vavassori, J. Nogues, B. Sepulveda, Simultaneous local heating/thermometry based on plasmonic magnetochromic nanoheaters, Small 14 (2018), 1800868-1–1800868-10.
[60] J. Lojk, V.B. Bregar, K. Strojan, S. Hudoklin, P. Veranič, M. Pavlin, M. Erdani Kreft, Increased endocytosis of magnetic nanoparticles into cancerous urothelial cells versus normal urothelial cells, Histochem. Cell Biol. 149 (2018) 45–59.